SETSCI Conference Proceedings,
4 (1): 603-611, 2019

ISAS 2019
3rd International Symposium on Innovative Approaches in Scientific Studies
Section: Engineering and Natural Sciences
April 19 – 21, 2019, Ankara, Turkey

Aerodynamic Analysis of Flow over a Pitching Airfoil

Veli Aşıcı[1*+], Murat Erbaş[2] and Atilla Bıyıkoğlu [3]

[1,2,3]Mechnanical Engineering/ Department of Engineering, Gazi University, Ankara, Türkiye
[*]Corresponding author, [+]Speaker: veli.asici@gazi.edu.tr
Presentation/Paper Type: Oral / Full Paper

Abstract – This study aims to investigate the effect of pitching motion of a NACA 0012 airfoil on the lift and drag coefficients at different reduced frequencies for a flow over the airfoil at Reynolds number of $5x10^5$. A two-dimensional computational analysis was performed for the airfoil at standard sea level conditions and reduced pitching frequencies of 0.1, 0.5 and 2.0 for the amplitudes of 20 degree and 30 degree with a mean incidence angle of zero degree. Besides, the effect of the flow velocity on the aerodynamic loads over the airfoil for the laminar, turbulent and transition regions is investigated. Reynolds Averaged Navier-Stokes equations are used in the numerical study with fully structured quad lateral grid structure. k-ω SST transport turbulence model is adapted to capture turbulence effects. The numerical model is validated using the experimental results existing in the literature. The results show that there is a significant importance of reduced frequency of oscillation over the lift and drag hysteresis loop on graphics.

Keywords – pitching motion, computational study, airfoil, lift coefficient, drag coefficient

1. INTRODUCTION

Oscillating airfoils, turbo machines, wind turbines and aerodynamic applications are investigated in many experimental and numerical analyses at different applications for civil and military fields [1]. The most important events in flow applications are on the separation of the flow and the dynamic stall where the flow rate is reduced to zero. In these cases, the aerodynamic lift coefficients and the oscillation moments vary widely. Due to non-linear behavior of high-impacts, aerodynamic coefficients vary considerably through flow over pitching objects. The selected literature related to pitching effect is presented below:

In the study of Zakaria et al., they have tried different oscillation waveforms in sinusoidal, trapezoidal, saw tooth and reverse sawtooth forms in oscillating airfoils. In their study, they performed pitching tests at 3.5°, 7°, 12° and 3.5° angles of amplitude. In this study, the frequencies were determined as 0.025 and 0.140 and $Re=2.1x10^4$ corresponding to free stream speed of 4.7 m/s. In the experiments, they have tried to determine the effects of wave movements of an oscillating wing on lift and friction coefficients. The unstable aerodynamic responses measured were compared with those in the semi-stable and unstable state models. In the trapezoidal and reverse saw tooth wave form test, the loss of lift coefficient was observed less than the one in the other wave form tests. The study showed that different oscillating waves were created higher static lift responses than the one for non-oscillating cases.[2]

In the study of Ossman H. et al., they have examined the effect of reduced frequency on the flow area under the aerodynamic forces and the lift frequency response of a NACA 0012 airfoil pitching at different reduced frequencies. The wing profile was centered at a distance of 0.25 chord length, and was analysed with the computational fluid dynamics approach between 0.1 and 0.9 reduced frequency values. To compare the frequency response characteristics with the lifting response function obtained from the numerical approach, Theodorsen method was used as the analytical approach. The analyses were carried out for a free stream velocity of 8.6 m/s with an average angle of attack of 3° and an amplitude of 6°. At low and medium frequencies, the lifting amplitude is tended to decrease and lift delay is decreased with an increase of reduction frequency. On the other hand, the drag coefficient was observed steadily increased in both amplitude and the phase delay of the oscillation frequency. [3]

In the study of Ghoreyshi et al., they have investigated the challenges of unstable lift modeling in the transition to the high angle of attack of the two-dimensional NACA0012 wing profile. Numerical analysis has been performed at reduced frequencies of 0.1 and 1.0 for forced oscillations. The results from the computational fluid dynamics study show that changes in the lift angle varying with the coefficients of hysteresis and the shape of the loops are significantly affected by the reduced frequencies. In the oscillation and plunge motion with reduced frequency of k = 0.1, the dynamic stall vortex is detected. This vortex has determined that flow separation can be postponed to higher attack angles. With the compression wave on the bottom surface and the expansion wave on the upper surface, the formation of unstable lifting forces of very fast movements has been substantially ensured. The results show clear boundaries of unstable aerodynamic theories for motion modeling in high attack angles. [4]

The aim of this study was to reach to response effects of the airfoil pitching at reduced frequencies of 0.1, 0.5 and 2.0 for Reynolds number of 500.000. The effects of the pitching airfoil at a mean incidence angle and with various pitching frequencies were investigated over the aerodynamic loads and flow streamlines in the computational domain. The flow dynamics was investigated with CFD solver using Reynolds

Averaged Navier-Stokes equation. The solution of unsteady flow equations gives information about flow characteristics such as lift and drag coefficients, moment coefficient of flow. The instantaneous computation of transient equations provides information about instant aerodynamic effects and position of the airfoil at each time step. The mean incidence angle (α_m) and the two pitching amplitudes for the flow over airfoil were selected as 0° and, 10° and 15°. The grid structure of the computational domain was build up based on O-type grid. The computational domain with 6 m in diameter was concentrically divided into a sub-domain with 2.67 m in diameter. The outer domain was statically structured and the inner domain as dynamically. The chord length of airfoil was 0.375 m. It was positioned at the center of the computational domain with a distance of 0.25 chord-length from leading edge.

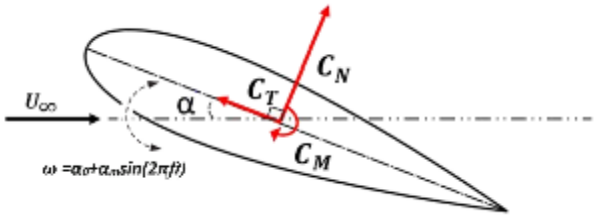

Fig. 1. Figure of the NACA0012 airfoil pitching sinusoidally at a center of the quarter chord point, with amplitude (Δα) and frequency(f) around a mean angle of attack(α_m) in a uniform flow (U) and the rotation formula is $\omega = \alpha_0 + \alpha_m sin(2\pi ft)$

Fig. 2. The 3-D geometry of NACA 0012 airfoil

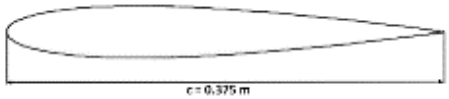

Fig. 3. The 2-D geometry of NACA 0012 airfoil

2. COMPUTATIONAL MODEL

2.1.Turbulence Modelling

In the flow over the airfoil, flow separation and vortex occur at high speed values of free streams. To be able to catch these phenomena accordingly, different turbulence models have been examined with the same boundary conditions in this study. Numerical analyses were performed using the turbulence models of Stable Laminar flow, Spalart-Almaras, k-ε realizable and k-ω SST. Expectation from these models is to model accurately the flow separations and combinations.

In the study of Swanson and et. al., they analysed stable laminar flow solutions with NACA 0012 wing profile. Laminar flow analyses are often used to control the accuracy, stability and convergence of numerical solution algorithms of Navier-Stokes equations. It is advised to invoke a hierarchy of laminar test cases in which they eliminate the need at sufficiently high Reynolds numbers to either resolve turbulence in a flow field or to model the turbulence appropriately. [5]

In Nae's article, k-ε turbulence model has been used as the solution approach due to the high turbulent kinetic energy emitted at the edges of the synthetic jet. The model gave fine results at a constant distance of y+ value of 200 for low Reynolds numbers. Standard and k-ε turbulence models were not adopted for this study, because they could not provide the correct solution in the analysis of flow separation.[6]

k–ω turbulence models have high sensitivity to inlet conditions and cannot provide converged solution for k-ε in trailing edge flows.

k–ε turbulence models give fine results through the boundary layer and leading edge, however the sub-layer models give less accurate and less complexity results. k-ω turbulence models give more accurate and sensitive results in sub-layer and freestream region. Consequently, the model is used as main turbulence model. k–ω SST (Shear Stress Transportation) turbulence model is formed by Menter by combining of k–ω ve k–ε models. This model is effective to detect the flow vortexes at moving leading edge at a wide range of Reynolds numbers. The model is selected to guess the flow separation which is important in aeronautical applications and to guess the adverse pressure gradient.

2.2. Governing Equations

The details of turbulence model formula and blending function calculation and solution can be found at Menter (1994).[7]

In the Shear Stress Transport model, Turbulence viscosity (ε_m) equation is given Eq.A.1. At this model, the turbulence viscosity is limited with F_2 parameter.[8]

$$\varepsilon_m = \frac{a_q k}{\max(a_1\omega; \Omega F_2)} \qquad (A.1)$$

$$F_2 = \tanh\left(\arg_2^2\right) \qquad (A.2)$$

$$\arg_2 = \max\left(2\frac{\sqrt{k}}{0{,}09\omega y}; \frac{500\nu}{y^2\omega}\right) \qquad (A.3)$$

In the Shear Stress Transport model, to compute the turbulence viscosity, the turbulence kinetic energy (k) at Eq.A.4 and specific dissipation rate (ω) Eq. A.5 are solved for cells.

$$\frac{\partial(\rho k)}{\partial\tau} + \vec{\nabla}\cdot(\rho\vec{V}k) = \vec{\nabla}\cdot[(\mu + \rho\varepsilon_m\sigma_k)\vec{\nabla}k] + \bar{\bar{R}}:\vec{\nabla}(\vec{V}) - \beta^*\rho\omega k \qquad (A.4)$$

$$\frac{\partial(\rho\omega)}{\partial\tau} + \vec{\nabla}\cdot(\rho\vec{V}\omega) = \vec{\nabla}\cdot\left((\mu + \rho\varepsilon_m\sigma_\omega)\vec{\nabla}\omega\right) + \frac{\gamma}{\varepsilon_m}\bar{\bar{R}}:\vec{\nabla}(\vec{V}) - \beta\rho\omega^2 + 2(1-F_1)\rho\sigma_{\omega 2}\frac{1}{\omega}\vec{\nabla}k\cdot\vec{\nabla}\omega \qquad (A.5)$$

Where $\bar{\bar{R}}$ stands for Reynolds Stress tensor and is presented below

$$\bar{\bar{R}} = \rho\varepsilon_m\left(\vec{\nabla}\vec{V} + (\vec{\nabla}\vec{V})^T - \frac{2}{3}\delta\vec{\nabla}\cdot\vec{V}\right) - \frac{2}{3}\mu k\delta \qquad (A.6)$$

At Shear Stress Transport (SST) k- ω type model, k-ε ve k-w models are modified according to F_1 parameter value as shown in Eq. A.7. When F_1 equal to 1, the model converts to k-ω and when F_1 equal to 0, the model converts to k- ε.

$$F_1 = \tanh\left(\arg_1^4\right) \qquad (A.7)$$

$$\arg_1 = \min\left(\max\left(\frac{\sqrt{k}}{0{,}09\omega y}; \frac{500\nu}{y^2\omega}\right); \frac{4\rho\sigma_{w2}k}{CD_{kw}y^2}\right) \qquad (A.8)$$

$$CD_{kw} = max\left(2\rho\sigma_{w2}\frac{1}{\omega}(\vec{\nabla}k\cdot\vec{\nabla}\omega), 10^{-20}\right) \qquad (A.9)$$

3. COMPUTATIONAL DOMAIN AND STRUCTURAL GRID

3.1. Computational Domain

Bounds of computation domain are defined in Fig.4. In the freestream flow area, the free flow rate is defined by specifying the static pressure values. At the flow inlet, the flow rate is fixed along the X axis, defined at 0 along the Y axis. Output section is defined as Pressure Output and its value is fixed as 0 pascal. No slip boundary condition is provided on the airfoil. At the point above the wing, the flow rate is defined as 0.

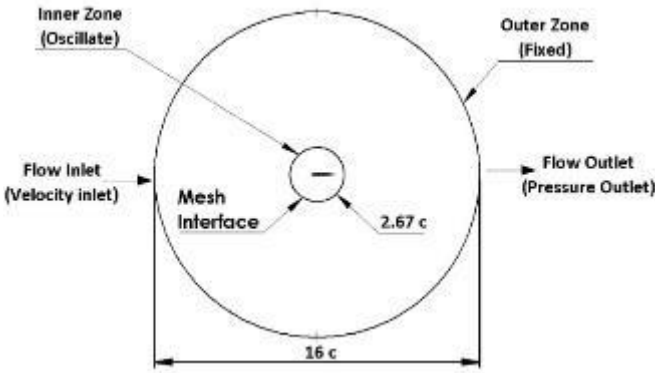

Fig. 4 Setup of Computational Domain

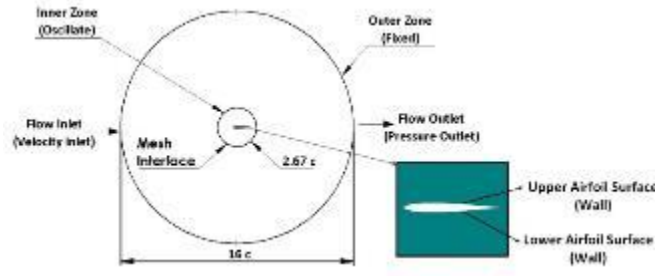

Fig. 5. Setup of Computational Domain

After, the divided interfaces are defined as conjugated. The inner domain formed with structural condensed with grid. The grid around the airfoil is shown at the Fig.9.

3.2. Structural Grid

The tetrahedral grid structure is shown for the flow modeling around the wing profile. Dynamic and Static area's grid number has been increased in the structural domain. The cells were compacted at the bottom of the wall so that the flow was in the laminar sub-region for the wall boundary condition.

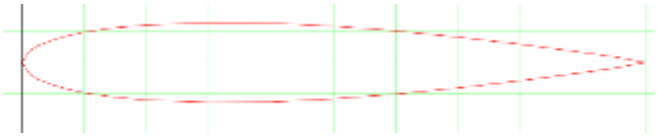

Fig. 6. NACA 0012 Wing Profile

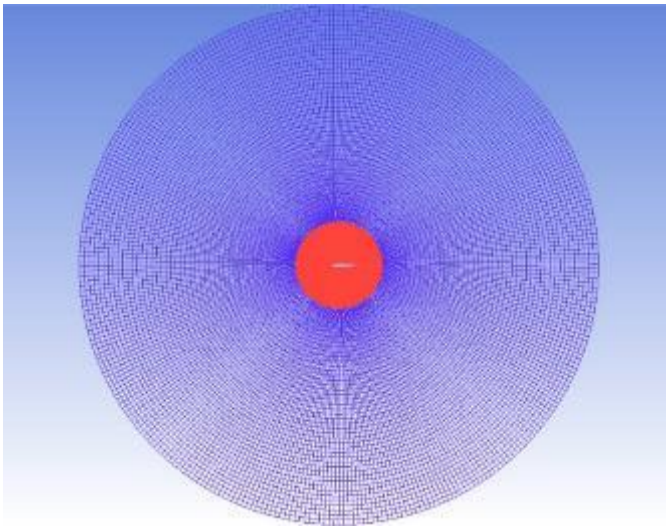

Fig. 7. Grid Structure at Computational Domain

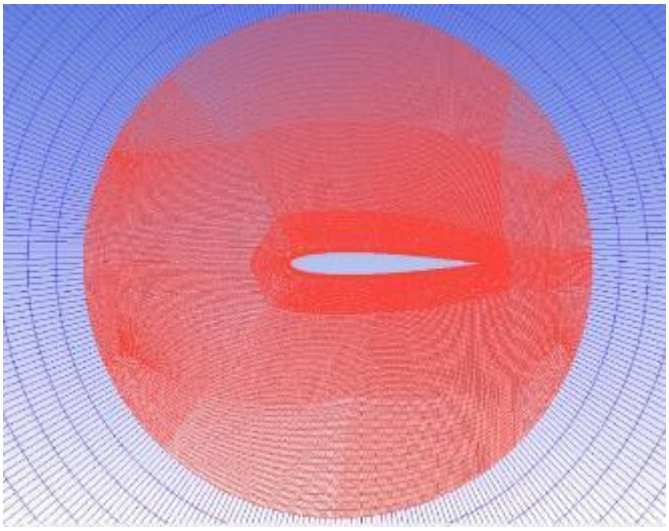

Fig. 8. Dynamic Domain Structural Grid

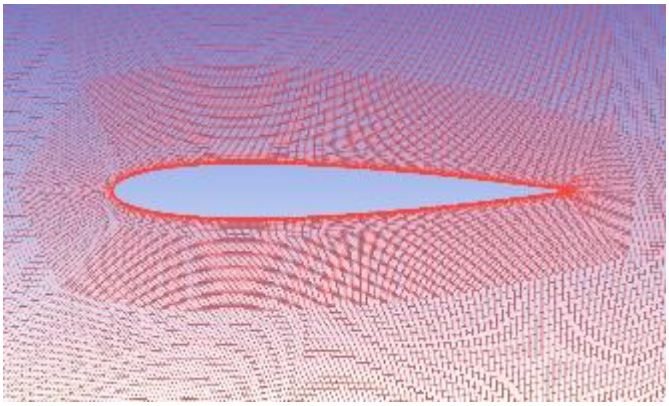

Fig. 9. Condensed Grid Structure around Airfoil

Table 1. Computational Domain Boundary Conditions

No	Boundary	Boundary Condition	Turbulence Boundary Condition
1	Inlet	Inlet Velocity 19,47646 m/s	% 0.01 Turbulence Intensity
2	Outlet	Outlet Pressure 101.325 kPa	%5 Turbulence Intensity
3	Wall	No Slip C=0	-
4	Interface	Conjugated	Conjugated

The flow analysis domain was formed by a non-structural grid around the wing profile. The flow domain was formed by a circular O-type structural grid with a diameter of 16 chord-length and a circular dynamic grid structure with a diameter of 2.67 chord-length to the computational domain. In the area of oscillation, the center of dynamic domain grid structure was determined as 0.25 chord length from the starting point of the wing profile leading edge. The external computing grid structure is consistently and structurally formed and the outer layer is divided into x-axis alignment to define flow input-output conditions.[9]

While the external structural grid domain is included in the calculations, the wing profile in the dynamic non-structural grid domain and the oscillation function equations around the center of 0.25c are given below.[10]

Pitching angular velocity; $\omega=\alpha_0+\alpha_m sin(2\pi ft)$

Reduced frequency; $k=\pi fc/U$

In this formula, α_0, α_m, ω, f, k, U terms designate the oscillation period, the mean angle of attack, the radial frequency [rad/s], the operating frequency [Hz], the reduced frequency and freestream velocity [m/s], respectively. Oscillation frequency was determined from the dynamic field center with a diameter of 2.67c and numerical studies were performed at different frequencies with UDF (User Defined Function).[3]

3.3. Grid Independence Test

In order to assess the quality of the grid, various grid sensitivity analyses were performed and verified. 9 different grid resolutions have been created. Grid resolutions; cell heights on the solid wall are shaped by the number of cells perpendicular to the wall. Numerical studies were carried out with 9 different grid structures in which all the same static conditions were applied. For constant Reynolds number of 200,000 and angle of attack of 0° conditions; k-ω SST turbulence model has been applied to all cases. The grid code 4, in which the change in drag coefficient between adjacent grid codes is 0.01%, is selected as the lowest grid number having independent solutions which eliminate unnecessary computational time.

Table 1. Results for different grid numbers

Grid Code	Total Elements	Nodes	Drag	Cd	Growth Rate	Y+
1	17668	17240	1,03917	0,01193	3,33%	1,00E-01
2	33144	32558	1,07645	0,01235	-0,14%	1,00E-01
3	57152	56364	1,07363	0,01232	0,12%	3,00E-02
4	78638	79581	1,07513	0,01234	-0,01%	1,00E-01
5	152724	154030	1,07709	0,01236	-0,20%	4,00E-02
6	251878	249965	1,08285	0,01243	-0,73%	1,00E+00
7	339354	341305	1,07975	0,01239	-0,44%	1,00E-01
8	488038	485522	1,08773	0,01248	-1,19%	1,00E+00
9	599512	607302	1,07497	0,01234	0,00%	1,00E-01

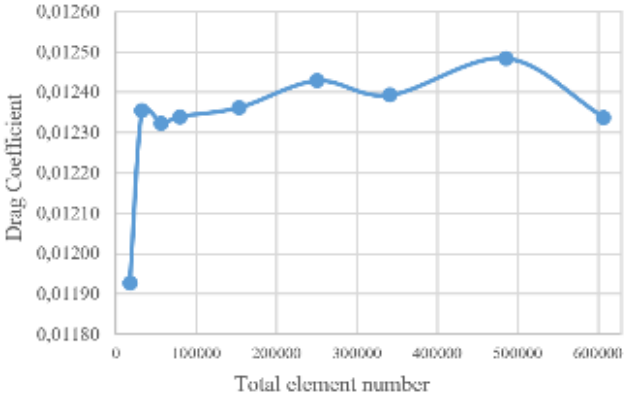

Fig. 10. Drag Coefficient and Total Element Number values graph

3.4. Validation of the CFD Solver

3.4.1. Laminar Case

Results of Sandiana Test for 'NACA0012H for VAWT' are used to validate the CFD solver at different Reynolds numbers. The results are compared and presented in Table 2 for five different Reynolds numbers creating similar conditions between the experimental and numerical cases at angle of attack of 0°. This enables it to evaluate only the effect of drag due to zero lift force when AoA is selected as zero. It is shown from Fig.11 that the numerical analysis results are well matched with experimental results [11] especially for the Reynolds numbers higher than $5x10^5$ and lower than $2x10^5$.

Table 2. Comparison of experimental and numerical results

Laminar Model, AOA=0°		Numerical Results		Experimental Results
Reynolds	V (m/s)	Drag Force (N)	Cd	Cd
1.000.000	38,9	2,40620	0,00690	0,00717
500.000	19,5	0,68630	0,00788	0,00688
200.000	7,8	0,15793	0,01133	0,00961
100.000	3,9	0,05716	0,01640	0,01642
50.000	1,9	0,01723	0,01978	0,02085

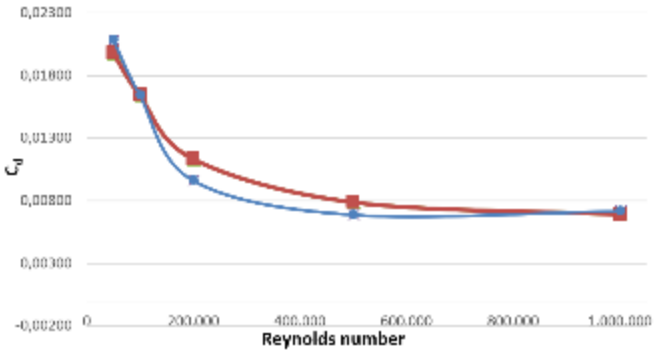

Fig.11. Comparison of experimental and numerical results for drag coefficient vs. Reynolds number

3.4.2. Oscillation Case

The oscillating case of this study is compared with the Kim et. Al.'s experiment which investigates the lift coefficient versus angle of attack at reduced frequencies of 0.1. For the validation of oscillation case, the conditions of Kim's experiment are stated as 0.1 of reduced frequency, Reynolds number $4.8x10^4$ at an amplitude of 6° at a mean

incidence angle of 0°. The results of this study and the experiment are shown in Fig. 12. The graph explains that uncertain conditions cause a sudden rising and lowering at lift line, however the general lift slope according to the angle of attack show similar arise over the whole pitching cycle. It can be concluded that the studied model is in good agreement with the experimental one. [12]

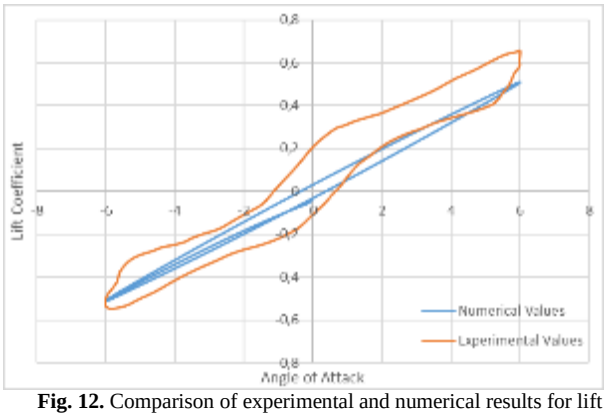

Fig. 12. Comparison of experimental and numerical results for lift coefficient vs. angle of attack

In the work of Marongiu, the three stall conditions have been examined such as a pre-stall, a light stall and a deep stall. The analysis occurred at $1.35x10^5$ Reynolds number with a reduced frequency of 0.05 at a mean incidence angle of 0° and the amplitude of pitching is 15° from -7.5° to +7.5°. The hysteresis of the coefficient of drag demonstrates a good adaption with the theoretical values. In this study, the results give us a smooth approximation between Marongiu computation and numerical study which was applied at the same flow conditions. The graph in Fig. 13 shows that the model was structured properly to give expected results. [13]

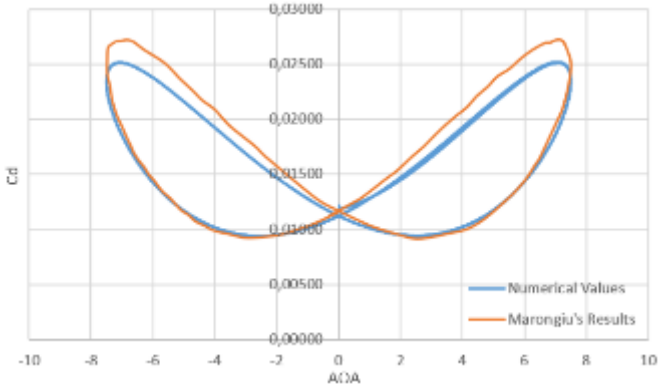

Fig. 13. The graph of drag coefficient vs. angle of attack

4. RESULTS

4.1. Lift and Drag Coefficient Analysis with different Reduced frequencies

At this study, three cases are investigated at reduced frequencies of 0.1, 0.5 and 2.0 to see the influence of the increasing and decreasing reduced frequency over a pitching airfoil by evaluating the force coefficients and flow figures of numerical results. The results of the cases have been illustrated in Figs. 14 and 15. The flow figures of several instants are supplied with respect to angle of attack. The figures show several type of plots as aerodynamic force coefficients, velocity vectors of flow and streamlines.

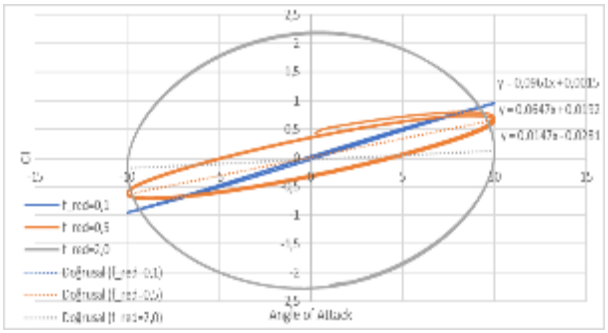

Fig.14. Lift Variation for reduced frequencies at 0.1, 0.5, and 2.0 for α_0=0˚, α_m=20˚, and U=19.47 m/s

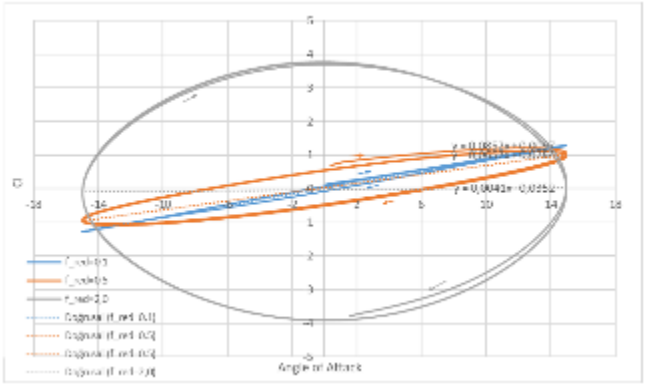

Fig.15. Lift Variation for reduced frequencies at 0.1, 0.5 and 2.0 for α_0=0˚, α_m=30˚and U=19.47 m/s

The results of the lift coefficient of entire oscillation motion cycles are compared for different reduced frequencies in Fig.14. The arrows through right direction show the upward pitching and others show downward direction of pitching motion. The lift values are plotted at a range of angle of attack from -10 degrees to 10 degrees. The graph in Fig. 14 shows that the amplitude of the lift coefficient also rises with reduced frequency.

It can be concluded from the numerical analysis of two different amplitudes that the aerodynamic loads are higher when the amplitude angle gets larger at each incidence angle. If the max. value of both lift and drag are compared, it is seen that the higher amplitude angle gives higher value for aerodynamic coefficient. The slopes of lift at different amplitudes changed conversely. It is seen from the both graph that there is no flow separation from the boundary layer. It is expected that when the flow separation occurs, the pressure decreases over the airfoil surface. It directly changes the load capacity of airfoil. Abrupt changes of the trailing edge angle because of the pitching motion create loss of lift. When the pressure distribution is examined through the airfoil surface, it is easily seen that the overdose changes of pitching reduced frequency, the lift start to decrease from the max. level of lift because of converse pitching motion.

The pitching frequency affects the maximum lift coefficient at both upstroke and downstroke motion. Because of the symmetry of airfoil, motions of upstroke and downstroke give the similar aerodynamic values. The lift changes very directly according to angle of attack when the reduced frequency equal to 0.1, The lifting forces guesses can be made more easily rather than the others. While the reduced frequency arises, the lift amplitude also increases at higher then frequency rating. The graph shows us that the max. and min. lift coefficient are affected by reduced frequency. The

slope of the lift shows a degressive rate with increasing reduced frequency.[14]

There is also an interesting response of the lift coefficient with comparison of a statical airfoil analysis/experiments. Because of finite time to develop the vortex structure at area where close to trailing edge, there is lag at lift coefficient according to the angle of attack. Figure gives a general idea to explain this situation. The larger reduced frequency gets, the bigger the lag value get. [15] The lift values of 0 is waited to reach at the angle of attack of 0°, however the 0 value of lift coefficient is seen to reach at higher than 5° angle. It shows the time dependency of the oscillating.

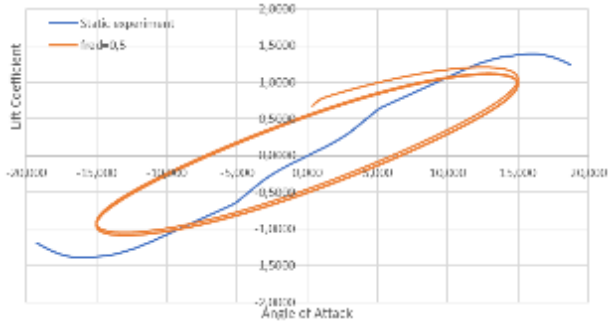

Fig.15. Lift coefficient comparison of numerical analysis with 0.5 reduced frequency and statical analysis incident angles of attack

The circularity of the lift rises with increasing reduced frequencies. The lift rate decreases while closing the limit degree of angle of attack. The incline of the lift which close to limit attack angle does not show a sudden changing negatively, it means that there is not a flow separation at this situation.

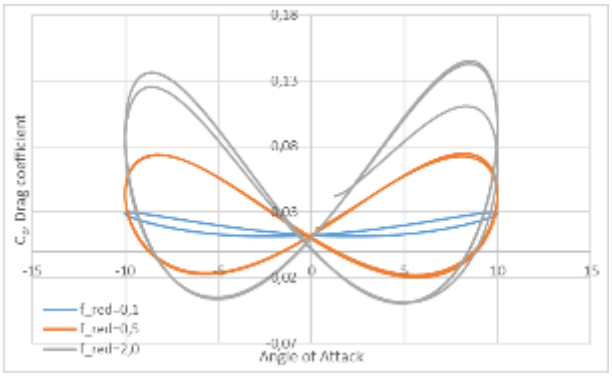

Fig.16. Drag Variation for reduced frequencies at 0.1-0.5-2.0 for α_0=0˚, α_m=20˚, and U=19.47 m/s

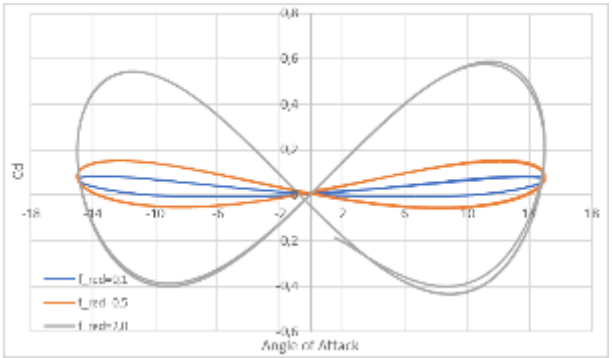

Fig.17. Drag Variation for reduced frequencies at 0,1-0,5-2,0 for α_0=0˚, α_m=30˚, and U=19.47 m/s

From the above plotting, there is rise at the drag values with increasing reduced frequencies. While loop closing the limit angle of pitching, hysteresis rotation loop width shows higher tightening while reduced frequencies decreasing.

When the angle of attack closes to the 0°, each reduced frequency pitching motion gives the approximately same values of drag coefficient value. If the max. C_d values are examined, it is seen that the difference for higher rate reduced frequency is larger than the others. When the upstroke and downstroke pitching max. drag coefficient is examined.

Adversely the changing reduced frequency gives a general idea for shaping the aerodynamic forces and moment of pitching, it does not explain accurate guesses for flow separation. It cannot be evaluated appropriately with force and moment values. The pressure distribution is the key role over the flow separation. Because of the changing the pressure distribution from leading edge to trailing edge, a suction pressure occurs. The values of the upstroke motion pressure distribution over upper and lower faces are higher than the values of the values of down stroke motion pressure distribution at any incidence angle. Also, the general smooth decreasing does not change with the variable reduced frequencies.[16]

The graph of pressure distribution show three cases for reduced frequencies. Because the flow separation occurs closer to 15° than 10°. The pressure distribution versus spanwise position through the airfoil surfaces values are plotted at different reduced frequencies.

4.2. Flow Streamlines at Dynamic Computational Domain

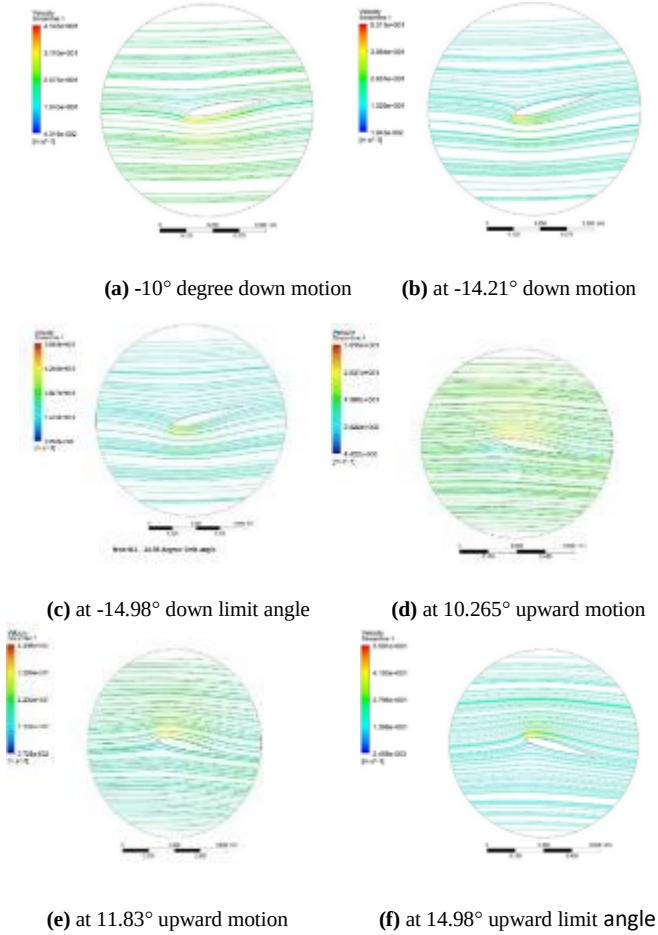

(a) -10° degree down motion **(b)** at -14.21° down motion

(c) at -14.98° down limit angle **(d)** at 10.265° upward motion

(e) at 11.83° upward motion **(f)** at 14.98° upward limit angle

Fig. 18. Down-stroke and up-stroke motion of NACA0012 with 0.1 Reduced Frequency oscillation of motion at a mean incidence angle of 0° with an amplitude of 15° at 500.000 Reynolds number

Fig.18 shows the flow streamlines visualization at $5x10^5$ Reynolds number with respect to different angle of attacks at a fixed reduced frequency pitching motion. The figures also show information about the flow characterization. The flow is regular over the airfoil at 0.1 reduced frequency. The flow streamlines around the airfoil makes any reversal flow motion and consequently, it is seen that there is not flow separation. During a cycle of pitching motion, the pre-stall condition does not occur at $5x10^5$ Reynolds number at a reduced frequency of 0.1 while the pitching motion is centered at a 0.25 chord-length from leading edge.

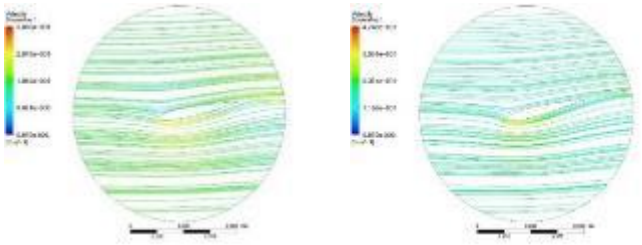

(a) at -11.08° downward motion **(b)** at -14.22° downward motion

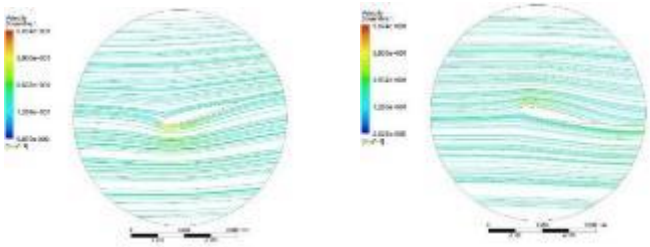

(c) at -14.94° downward motion **(d)** at 10.27° upward motion

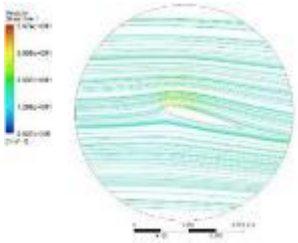

(e) at 11.83° upward motion

Fig. 19. Down-stroke and up-stroke motion of NACA0012 with 0.5 Reduced Frequency oscillation of motion at a mean incidence angle of 0° with an amplitude of 15° at 500.000 Reynolds number

Fig. 19 shows the free streamlines around the airfoil at 0.5 reduced frequency for Reynolds number of $5x10^5$ vs. angle of attack. The pitching motion at *k=0.5* creates a smooth difference from *k=0.1* pitching motion. The flow shows a regularity over the airfoil surface. Similarly, there is not seen any counter flow over the airfoil so flow separation does not occur. However, when the airfoil reaches the limit angle, the free streamlines move more quickly than the lower *k* values oscillating motion because of the increasing of reduced frequency.

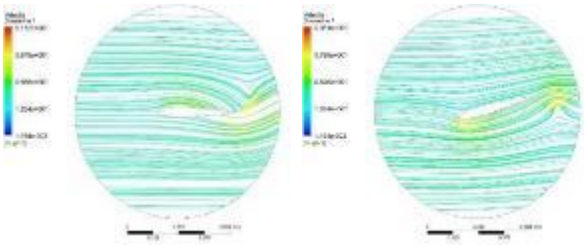

(a) at 0° downward motion **(b)** at -14.98° downward motion

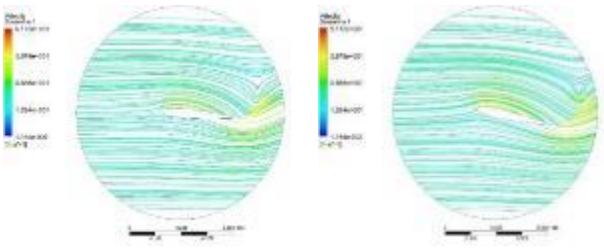

(c) at 5.2° upward motion **(d)** at 10.29° upward motion

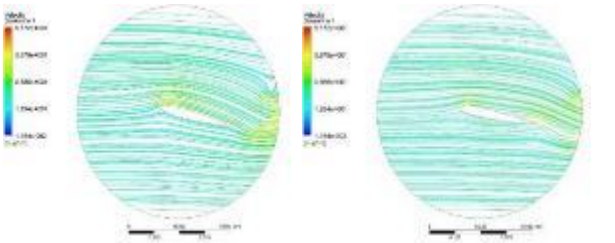

(e) at 14.98° upward motion **(f)** at 12.03° downward motion

Fig. 20. Down-stroke and up-stroke motion of NACA0012 with 2.0 Reduced Frequency oscillation of motion at a mean incidence angle of 0° with an amplitude of 15° at 500.000 Reynolds number

Fig. 20 shows the free streamlines around the airfoil at dynamic computational domain at *k=2.0* for Reynolds number of $5x10^5$ while pitching upstroke and downstroke motion cycle. The free streamlines demonstrate irregular flow because of the higher reduced frequency. However, the flow conditions do not allow flow to make reversal motions. Vortices cannot occur over the boundary layer. On the contrary, the vortex structures of flow are seen at far away from the wing profile. The pitching motion breaks down the flow streams. If the upstroke motion is examined, it is seen that the vortices which start from trailing edge to wake region formed at CW direction. The downstroke motion, of course, creates CCW vortex starting from trailing edge to wake region. The both converse motion before forming of flow streamlines decrease the flow energy and results in loss of lift and rising of drag motion.

4.3. Pressure Distributions over Airfoil Surfaces

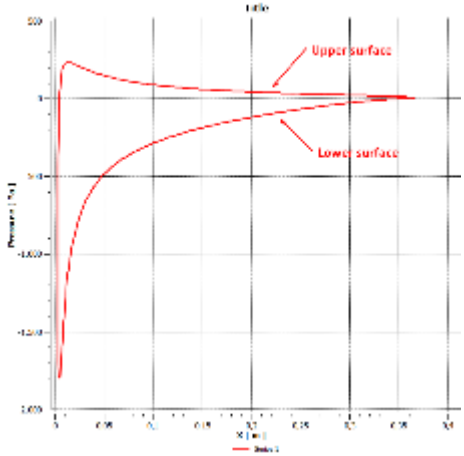

(a) Pressure distribution over airfoil upper and lower surfaces at 0.1 reduced frequency at 15° AoA

The figures show us the pressure distribution over airfoil surfaces when the airfoils are at positive 15° angle of attack. No sudden changes demonstrate the smooth changing of lift and drag through up-stroke and down-stroke motion. From the center of pitching motion, the difference pressure between the upper and lower surface declines, this means that the lifting value goes down.

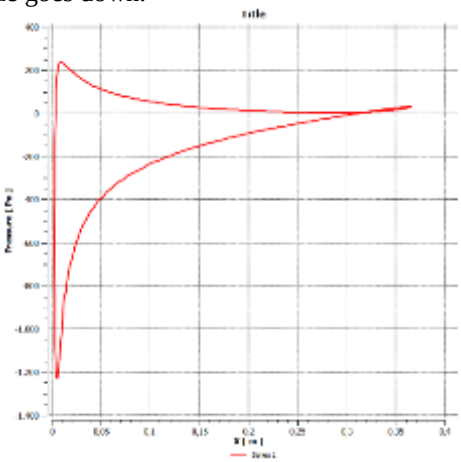

(b) Pressure distribution over airfoil upper and lower surfaces at 0.5 reduced frequency at 15° AoA

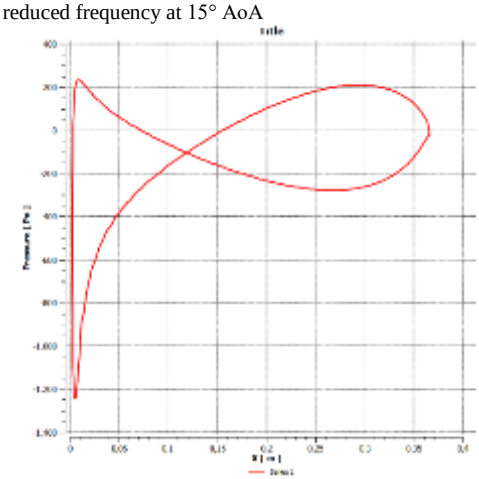

(c) Pressure distribution over airfoil upper and lower surfaces at 2.0 reduced frequency at 15° AoA

The situation shows the first sign at k=0.5 oscillating motion. The sign changes explain the decrease of lift from the max. lift coefficient in a quick way. The sign changes of pressure is close to the trailing edge at k=0.5 pitching motion. At k=2.0 pitching motion condition, the reverse motion which decline the lift is close to center of pitching. The max lift coefficient is higher at k=2.0 condition than other pitching motion, therefore the airfoil starts to lose at a higher lift value to lower level of lift.

5. CONCLUSION

In this paper, the reduced frequency effect over pitching airfoil was investigated for Reynolds number of $5x10^5$ under the effect of AoA amplitudes of 20° and 30°. The reduced frequencies of 0.1, 0.5 and 2.0 are applied to amplitude of pitching motion. At each section, the flow was visualized with respect to angle of attack during oscillating through both upstroke and downstroke movements. The visualizations of flow were organized chronologically according to pitching motion steps. From the visualizations, the CW and CCW direction vortices are gained at the k=2.0 at the wake region. There is no separation over the surfaces. It could be resulted from the high Reynolds number effect and delaying of separation to higher angle of attacks. Both lift and drag coefficients show nonlinear trace with respect to angle of attack. The pressure distribution over airfoil surfaces is examined at 15° AoA for each reduced frequency. The graphs demonstrate that the pressure distribution is more likely to statical analysis case at lower frequency. When the reduced frequency gets higher, the lines of pressure over surfaces differentiate from static case. The hysteresis of lift and drag coefficients is directly affected from the increasing of reduced frequency, as a result the max lift and drag coefficient increase non-linearly.

6. REFERENCES

[1] Farouk Ziane,Abdellah Abdellah El-Hadj,Arab J Sci Eng,,"Numerical Analysis of the Wall Effect on Flow Around Airfoil Subjected to a Pitching Movement", in DOI 10.1007/s13369-017-2701-12017

[2] Hisham M. Shehata, Mohamed Y. Zakaria, Y. Muhammad R. Hajjz and Craig A. Woolsey, AIAA Scitech 2019 Forum, "Aerodynamic Response of a NACA-0012 Airfoil Undergoing Non-Sinusoidal Pitching Waveform",2019

[3] M. Ossman H,M Y M Ahmed and M. Y. Zakaria, AIAA SciTech Forum,2018 AIAA Aerospace Sciences Meeting ,"Investigating the Aerodynamic Loads and Frequency Response for a Pitching NACA 0012 Airfoil",2018

[4] "Mehdi Ghoreyshi, Russell M. Cummings, Modeling and Simulation Research Center, U.S. Air Force Academy USAF Academy, Colorado 80840-6400,"Challenges in the Aerodynamics Modeling of an Oscillating and Translating Airfoil at Large Incidence Angles",2012"

[5] R.C.Swansona, S.Langer,"Steady-state laminar flow solutions for NACA0012 airfoil ", Computers and Fluids 126 (2016) 102–128.

[6] Catalin Nae,'' Unsteady Flow Control Usıng Synthetıc Jet Actuators'', American Institute of Aeronautics and Astronautics, AIAA-2000-2403,2000

[7] Menter, F. R. (1994), "Two-Equation Eddy-Viscosity Turbulence Models for Engineering Applications", AIAA Journal, vol. 32, no 8. pp. 1598-1605.

[8] Murat ERBAŞ, "The Aerothermodynamical Design and Simulation of Radial Turbines Used in Low Temperature Organic Rankine Cycle'', M. Sc. Thesis Gazi University Graduate School of Natural and Applied Sciences ,2016

[9] "Masoud Kharati Koopaee,"Effect of flow regime change from subsonic to transonic on the air loads of an oscillating airfoil", Journal of Fluids and Structures 50(2014)312–328"

[10] Jianping Niu, Juanmian Lei, Tianyu Lu, "Numerical research on the effect of variable droop leading-edge on oscillating NACA 0012 airfoil dynamic stall", Aerospace Science and Technology 72(2018)476–485

[11] Sandiana Test for 'NACA0012H for VAWT' " (Online), Available: http://airfoiltools.com/airfoil/details?airfoil=naca0012h-sa

[12] "Dong-Ha Kim, Jo-Won Chang, "Low-Reynolds-number effect on the aerodynamic characteristics of a pitching NACA0012 airfoil", Aerospace Science and Technology, Volume 32, Issue 1, January 2014, Pages 162-168"

[13] "Claudio Marongiu, Renato Tognaccini,"Simulation of the Dynamic Stall at Low Reynolds Number",48th AIAA Aerospace Sciences Meeting Including the New Horizons Forum and Aerospace Exposition, 4 - 7 January 2010, Orlando, Florida"

[14] Visbal,M.R., Shang,J.S., ''Investigation of the flow structure around a rapidly pitching airfoil'',AIAAJournal27,1044–1051,1989

[15] [Lorber PF, Covino Jr AF, Carta FO. Dynamic stall experiments on swept three-dimensional wing in compressible flow. AIAA Paper 1795, January 1991.]

[16] "Farooq Umar, Hossein Raza Hamdani, Anwar-ul-Haque, Sajid Raza Chaudhry and Khalid Parvez, "CFD analysis of an oscillating wing at various reduced frequencies'. J. Numer. Meth. Fluids 2009; 59:173–194"